Physical properties of the swept arc channel in the context of lightning strikes to aircraft

Vincent Andraud, R Sousa Martins, Clément Zaepffel, Romaric Landfried, Philippe Teste, Philippe Lalande

Physical properties of the swept arc channel in the context of lightning strikes to aircraft

V Andraud[1], R Sousa Martins[1], C Zaepffel[1], R Landfried[2], P Testé[2] and P Lalande[1]

[1]DPHY, ONERA, Université Paris Saclay, F-91123 Palaiseau, France
[2]Laboratoire GeePs, CNRS UMR8507, Université Paris Saclay, CentraleSupélec, 91190 Gif-sur-Yvette, France

E-mail: rafael.sousa_martins@onera.fr

Abstract

During an in-flight lightning strike, the relative motion between the arc channel and the aircraft causes a sweeping of the attachment point on the aircraft skin. To predict the behaviour of the arc channel and therefore the potential locations for further restrikes, this study aims at investigating the phenomenon with an innovative method for producing sweeping arcs based on a stationary arc and an electromagnetic launcher propelling aeronautical samples. This article focuses on characterisation of the arc channel, aiming at establishing the evolution of its physical properties during swept-stroke for various experimental conditions. Firstly, the experimental coupling of the lightning generator with the electromagnetic launcher and with a wind tunnel is described with a discussion on the representativeness of the experiment. Then, high-speed cameras and voltage and current probes are used to measure the electrical and geometrical behaviour of the electric arc channel during a swept-stroke. The shape, the length, the voltage and the power evolution of the arc channel are evaluated for different input parameters such as speed, polarity, arc current and sample length. Furthermore, the influence of these parameters on the temperature of the arc channel is studied, resorting to an optical emission spectroscopy technique. The results are presented and discussed with the objective of providing a physical insight into arc elongation phenomenology during a swept-stroke.

1. Introduction

Lightning is one of the most unrecognized and misunderstood of all common weather hazards and thus represents a critical challenge for flight safety. Damage to aircraft due to lightning strike occurs in the form of arc spots on the metal skin or centimetre-size holes in the fuselage. This risk is taken into account at the design stage of the aircraft since the phenomenon statistically occurs every 1000 to 10,000 flight hours, roughly one or two occurrences per year [1, 2]. As lightning strikes involve both a static lightning channel in the terrestrial reference frame and a moving aircraft – around 100 m s^{-1} for take-off and landing phases – there is a displacement of the arc spot on the aircraft's outer skin. This phenomenon is referred to as "swept-stroke". The displacement can be either continuous with the sweeping of the arc spot along the aircraft or discontinuous with the occurrence of arc root leaps [3]. Consequently, all parts of the aircraft are exposed to the risk of direct electrical and thermomechanical damage resulting from the passage of the arc root.

To ensure that an aircraft is able to endure a lightning strike, civil certification authorities (EASA, FAA) require from airplane manufacturers to conform to recommendations about lightning protection. Those recommendations are met through normative documentation established by standard committees such as EUROCAE and SAE. The recommendations present a standard current waveform defined in documents ARP5412A [4] and ED-84A [5] that stand for the upper limit of the different components of measured lightning currents. This standard current is composed of four current waveforms named A, B,

C and D as depicted in figure 1. The A, B and D components refer to pulse current phases (represented with a bi-exponential current with a 200-kA maximum peak amplitude and a time constant of few hundreds μs) whereas the C component reproduces the continuous phase (represented with a DC current of 200 to 800 A and a time constant from 250 to 1000 ms). Since the pulsed components durations are too short compared to the lightning arc root dwell time on an airplane surface point – from 1 to 20 ms [6] - it is commonly accepted in numerical [7 - 9] and experimental works [3, 10] that only the continuous component has to be considered to study the swept-stroke phenomenon.

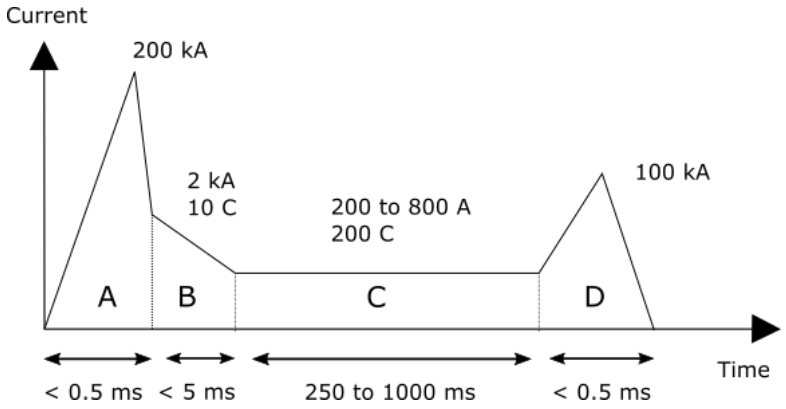

Figure 1. The standardized lightning current waveforms.

Different approaches have been taken to reproduce experimentally the swept-stroke phenomenon. As the phenomenon involves a relative motion between the arc channel and the material sample under test, experimental approaches can be divided into two main categories: settings that place the material sample in motion through a static arc channel and settings that place the arc channel in motion along the static material sample. Moving the arc can be achieved using transverse airflow from a wind tunnel or using rail electrodes and external or self-induced magnetic fields. Since the mass of an air heat plasma is negligible compared to that of an aeronautic material sample, such approaches may seem easier to implement even though techniques for controlling the air profile flow or the magnetic field require considerable precaution.

Several swept-stroke experiments resorting to wind tunnel techniques are reported in the literature [11 - 13]. However, wind tunnel experiments may seem unrealistic for the comprehension of the phenomenon and the relevance of the measured data for three main reasons. First, the arc sweeps across both electrodes so that both arc roots are moving and are subject to the same sweeping phenomenon, which could change the dynamic of the arc channel displacement. In reality, the lightning channel is stationary in air and only the part in the very vicinity of the aircraft surface is affected by the relative velocity. Second, the air flow is likely to cool the arc channel and thus add thermal constraints that could change the physical characteristics of the arc. Third, since the displacement of the arc channel consists in a heat and state change of the surrounding air to plasma involving electronic recombination processes, the energy balance is different in the configuration where the entire channel is blown and moves compared to the configuration in which only a segment of the arc plasma in the vicinity of the aircraft surface elongates. Magnetically driven arcs present similar problems to wind tunnel tests and external magnetic fields may also induce supplementary magnetic pressure constraint effects that could skew the dynamics of the arc column. Experiments using magnetic self-induced forces to move the arc channel and external magnetic forces are reported in the literature [10, 14, 15].

A moving surface test setup leads to simulations that are more representative of real lightning strikes on aircraft. The main drawback of these simulations is the relatively high speed to reach – up to

100 m s^{-1} – to be consistent with an aircraft velocity during a take-off or landing phase where the probability of being struck by lightning is the highest. Moreover, supposing such a speed is achieved, the acceleration distance that is required to propel test samples from 0 to 100 m s^{-1} is likely to be much greater than the normal dimensions of an experimental laboratory. The literature provides different approaches for simulating a moving surface [3]. The experiments that reached the highest speeds were the ones involving a rocked sled on a track using chemical propellant in Dobbing and Hanson [10]. In their work, the samples can reach a speed of 72 m s^{-1}, and are impacted by an arc that could be elongated to 5 m with a mean current of 600 A for up to 3s. Their paper presents current and voltage measurements and video recordings from which lengths and dwell times are directly obtained. Tests with bare metal, carbon fibre and painted protection are reported and give experimental data that are widely used for numerical simulations as validity criteria [7, 8, 9, 16, 17]. But the main problem of this latter experiment is the lack of accurate electrical and optical measurements, which is a limit for obtaining further physical characteristics of the arc column and its interaction with the sample surface.

A third category of testing method consists in direct in-flight measurements: an instrumented aircraft flying through an area of storm clouds. Frequent flight research programs have been conducted [18-21] and have contributed to feeding databases for statistical analyses [16, 22]. However, even though such tests are more representative than ground experiments, there are still major problems for building a robust and reliable database. First, it is not possible to control the experiment features: there is no control of the lightning channel parameters and it is quite impossible to obtain accurate electrical and optical measurements to characterise swept-stroke phenomena and plasma interactions on the aircraft surface. Second, the cost of such experiments is not negligible and represents a limit for good repeatability.

Thus, no significant experimental measurements of the swept-stroke phenomenon have produced physical characterisation of arc behaviour during swept-stroke in order to provide inputs or to serve as comparison to simulation codes for their validation. There is also no reference database demonstrating the likely evolution of swept-stroke quantities of interest taking into consideration the relevant experimental conditions. This lack of experimental results is currently provoking an issue with the validation of the developed models for computational simulation tools. Indeed, the computational simulations presented in the most recent papers, taking into account complex MHD [9] models and turbulent instabilities, [23] predict severe conditions for reattachment to occur that are in contradiction with the experimental measurements. Therefore, existing tools for the prediction of the location and the amplitude of the damage induced by the moving arc spot do not make it possible to design accurate and optimised protections that minimise aircraft weight while ensuring its endurance and resistance to lightning strikes. It is also important when designing further experimentation and protection tests to determine the impact of the mode of relative motion – moving arc or moving test sample – on the physical processes occurring during swept-stroke.

To establish a relevant experimental database fulfilling the scientific needs, the present study uses the experimental instruments developed in two recent papers: a DC lightning generator [24] and a railgun electromagnetic launcher [25]. These two instruments are coupled to reproduce a swept-stroke experiment. The main objective of this paper is to study the spatial elongation, the voltage evolution and the temperature of the arc channel during swept-stroke. Section 2 aims to present the experimental setup that makes it possible to study swept-stroke in a laboratory infrastructure for a moving test sample with the railgun facility and a moving arc with wind tunnel equipment. Section 3 is dedicated to describing the phenomenology of swept-stroke depending on the nature of the relative motion between the arc and the test sample. In section 4, the different experimental results concerning the electrical and thermal characteristics of the arc channel are presented. Then, section 5 discusses the influence of the experimental parameters on the physical characteristics of the arc channel during swept-stroke.

2. Experimental Setup and Test Matrix

2.1 Description of the test equipment

In order to produce a lightning swept-stroke in the laboratory, there is a need for:

- A lightning generator capable of reproducing electric arcs respecting the lightning arc waveform as defined in aeronautical standards.
- A launcher instrument capable of propelling aeronautical test samples inside a laboratory at speed levels characteristic of aircraft take-offs and landings.

The lightning arc generator used in this work is capable of producing electric arcs of up to 1.5 m with a current regulation of 200 to 800 A, respecting the C* standard aeronautical lightning waveform described in SAE ARP5412B [26] and ED 105A [27]. It is described in Andraud *et al.* [24].

The railgun equipment used in this work is described in Andraud *et al.* [25]. It is able to propel aeronautical test samples of weights between 100 and 250 g to speeds between 40 and 80 m s^{-1} within 2 m of acceleration. The coupling of this instrument with the lightning arc generator is presented in figure 2 with a representation of the different steps. The experiments using the railgun to propel aeronautical test samples through an electric arc are referred to as RGE in the present paper. More details about the coupling can be found in [28].

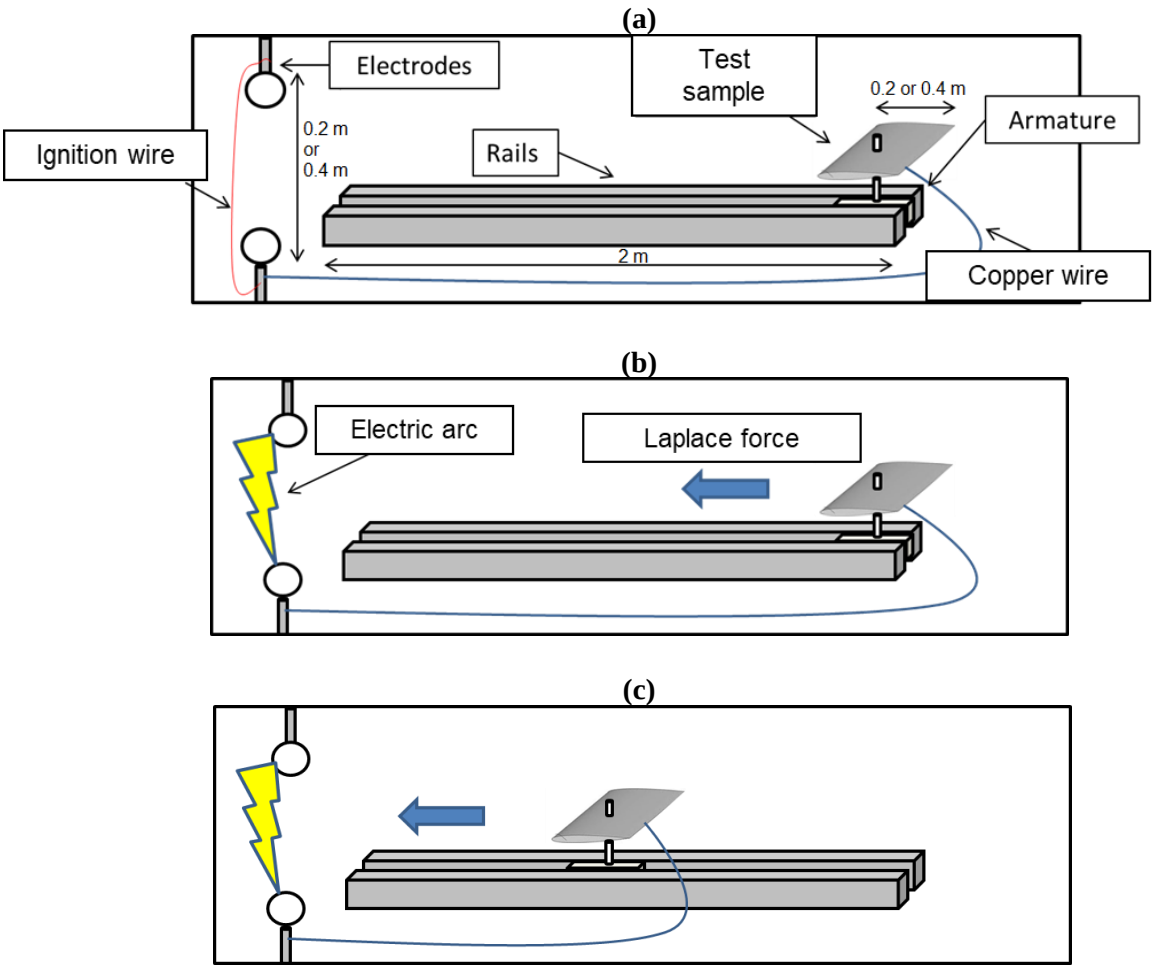

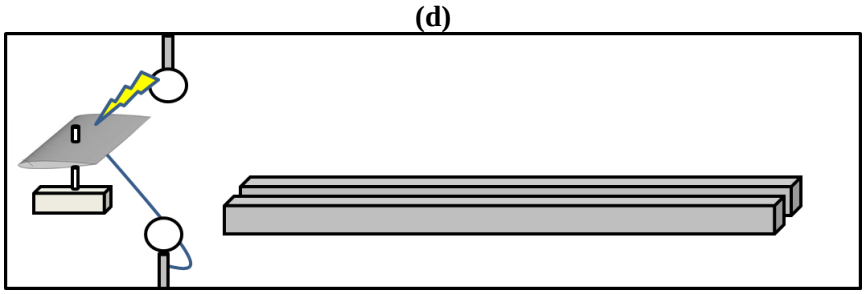

Figure 2. Coupling of the lightning arc generator and the railgun equipment (a) The test sample is mounted on the armature placed between the rails and an ignition wire is placed between the generator's electrodes (b) the electric arc is triggered and a current is inserted in the rails provoking a Laplace force to the projectile (c) the projectile is accelerating (d) the projectile leaves the rails and is struck by the electric arc producing the swept-stroke. Schematic diagrams out-of-scale.

The wind tunnel used in this work is powered by a 15-kW motor from DELTALAB. An adapter of rectangular section is added at the exit of the wind tunnel to homogenise the outgoing flow. Its dimensions are 250 mm height and 175 mm width. The experiments using the wind tunnel to blow electric arcs on aeronautical test samples are referred to as WTE in the present paper. The coupling of this instrument with the lightning arc generator is presented in figure 3 with a representation of the different steps.

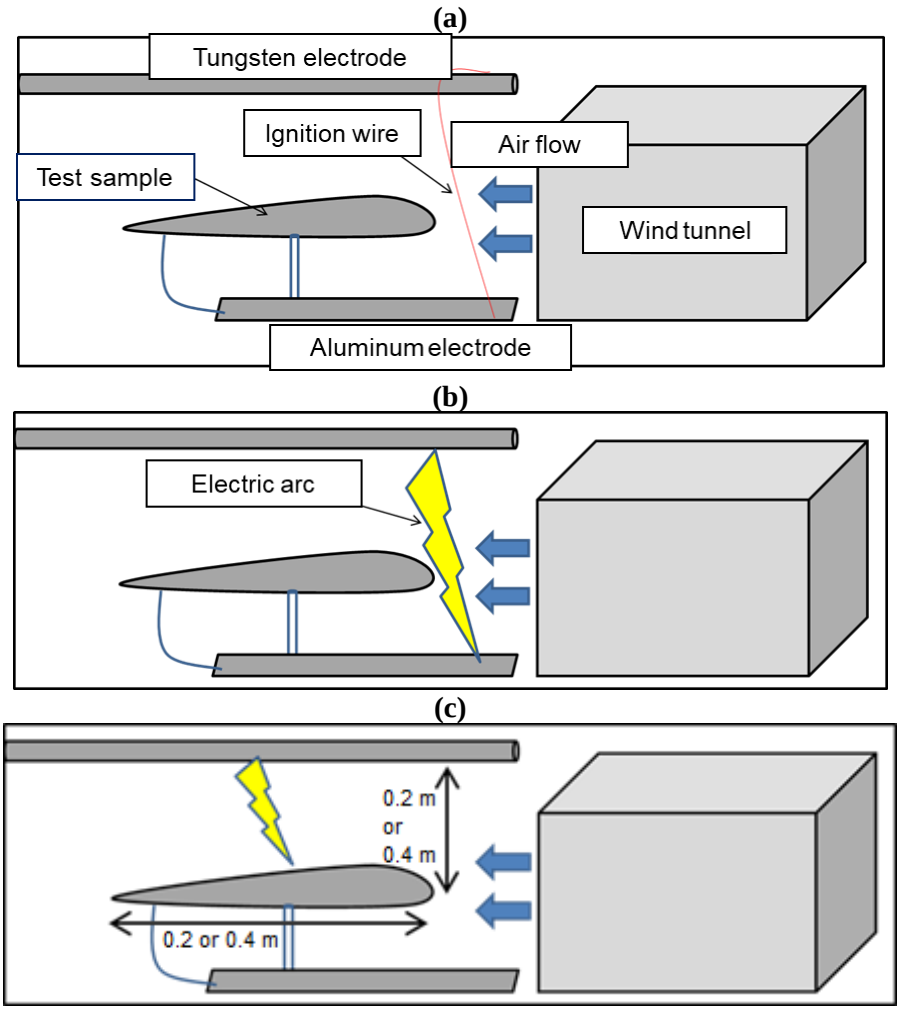

Figure 3. Coupling of the lightning arc generator and the wind tunnel facility (a) The test sample is placed at the muzzle of the wind tunnel and the flow is established (b) the electric arc is triggered and blown toward the test sample (c) the arc reaches the projectile thus producing the swept-stroke. Schematic diagrams out-of-scale.

The flow can be monitored for velocities up to 70 m s^{-1}. The projectiles launched with the railgun equipment are studied for speeds from 40 to 60 m s^{-1}. The wind tunnel facility is used for two flow velocities – 40 m s^{-1} and 60 m s^{-1}. In both configurations, to avoid the coexistence of two arc roots on the sample, it is directly connected to the ground or to the positive potential, playing the role of a cathode or an anode. The upper electrode is a horizontal rod of tungsten for RGE and a vertical one for WTE in order to allow the arc root to displace freely horizontally. The distance between the test sample and the upper electrode is adjusted to 200 mm in both experiments since the certification document ED-14E [29] recommends a minimum inter-electrode distance of 50 mm. Photos of the two setups can be found in [28].

2.2 Description of the sample geometry

The considered geometry for the test samples is the NACA 0012 profile. NACA airfoils are airfoil shapes for aircraft wings designed by the National Advisory Committee for Aeronautics (NACA). To create our samples, two resin models were built with a 3D printer. One has a chord of 200 mm and the other has a chord of 400 mm. These two lengths have been chosen to study the impact of the length of the sample in the swept-stroke phenomenon. The resin model with a 400 mm chord length is shown in figure 4 with an aluminium test sample reproducing this shape. In the railgun and in the wind tunnel experiments, panels of aluminium alloy 2024-T3 with a thickness of 0.4 mm are wrapped and stiffened around the model. Expanding foam is added within the sample to stiffen it during the acceleration phase. In the case of the wind tunnel facility, the plate of aluminium is fixed on the model and screwed onto a bulk table.

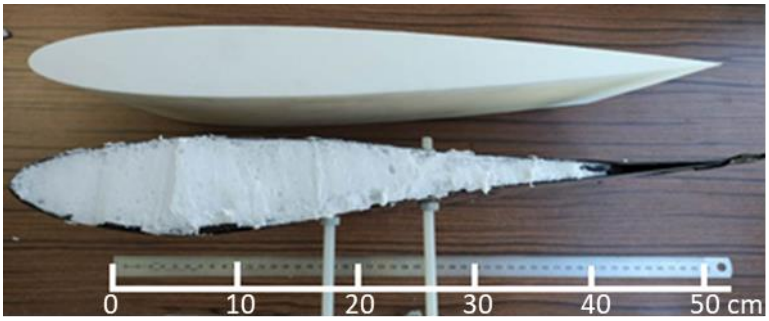

Figure 4. Picture of the railgun projectile with a NACA 0012 profile presenting a chord of 400 mm.

In real conditions of lightning strikes to aircraft, the surface of the aircraft is covered by paint. In this study, the only material considered is aluminium since our objective is to establish an initial database that will serve as a comparison for simulation codes. Thus, effects of the nature and thickness of the paint layer were not studied.

2.3 Description of fast imaging and electrical diagnostics

The current measurements are performed using a PEM CWT60LF probe. The voltage measurements are performed using North Star PVM-1 and Lecroy PPE5KV probes. The swept-stroke phenomenon is visualised using two high-speed cameras (HSC). The HSC are Phantom V711 from Vision Research. One camera is positioned transversely to the axis of the projectile movement in the case of the railgun

experiment and perpendicularly to the flow direction in the wind tunnel experiment and is adjusted to the height of the sample. This enables a 2D visualisation of the arc displacement perpendicular to the relative movement. However, the relative movement of the arc root is not entirely in a 2D plane, thus a second camera is positioned at an angle of 45° with the direction of projectile motion or the airflow. This camera is elevated above the height of the plane where the test sample is struck by the electric arc in order to provide additional information on the 3D elongation of the arc.

In RGE, the perpendicular camera was positioned to capture images composed of 704 × 160 pixels with a ratio of 1 mm pixel^{-1}. The interval between two pictures is 17.53 µs with an exposure time of 0.35 µs. In WTE, the perpendicular camera was positioned to capture images composed of 512 × 200 pixels with a ratio of 0.833 mm pixel^{-1}. The interval between two pictures is 15.87 µs and the exposure time is set to 1 µs. The second camera presents an inclined visualisation of the phenomenon: it is not scaled and only provides qualitative information. The interval between two pictures is 30.29 µs. Neutral-density filters (OD2) are used to avoid saturation in both cases. The two HSC are synchronised and enable an approximate 3D representation of the arc elongation.

2.4 Optical emission spectroscopy setup

Optical emission spectroscopy (OES) is employed in this work to observe the species present within the arc column as well as to estimate the arc temperature. The spectrometer used is an AvaSpec ULS3648 from Avantes (Symmetrical Czerny-Turner, 75 mm focal length, wavelength range from 200 to 1100 nm, CDD linear array with 3658 pixels, spectral resolution of 0.33 nm pixel^{-1} at 500 nm). The optical fibre is a fused silica, with a core of diameter equal to 200 µm and a numerical aperture of 0.22 that is connected to the spectrometer via an SMA connector. An optical setup is used for imaging a portion of the arc column at the entrance of the optical fibre. The optical setup is composed of a lens tube (0.5-inch diameter) that holds the SMA connector fibre, a fused silica lens with a focal length of 30 mm and a neutral-density filter (OD1). This setup is located 2 metres from the phenomenon, allowing the collection of a chord crossing the arc column. Figure 5 illustrates the experimental setup. The acquired spectra were calibrated in relative intensity using a DH-2000-CAL Deuterium Tungsten-Halogen Calibration Light Source from Ocean Optics.

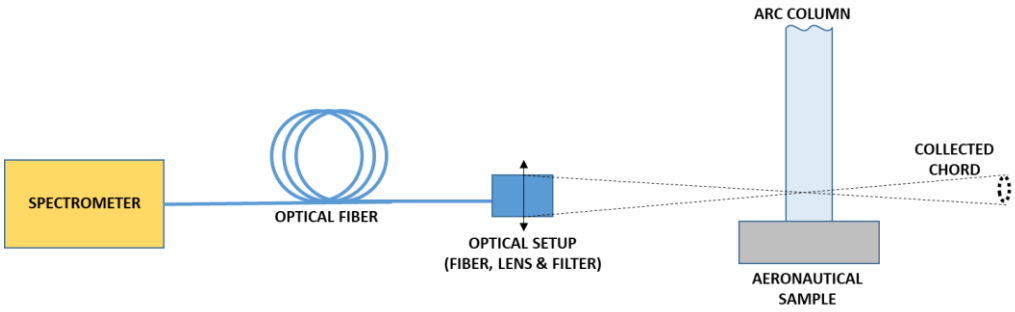

Figure 5. Experimental setup of OES measurements.

The positioning and size adjustment of the collected chord is done by analysing the spot of a laser beam following the reverse optical path. Synchronisation of the swept phenomenon with spectrum acquisition is very difficult, because the electrode/arc column is moving and we cannot know in advance when and where the arc will hang on the aeronautical sample. For that reason, we chose to use a large spot in the collected chord, with a spot diameter of 15 mm, which degrades the spatial resolution, but increases the probability of recording the phenomenon. The exposure time was set to 10 µs, which is the spectrometer minimum time, but it is fast enough when compared to the arc motion (less than 1 mm displacement for

the considered velocities). The chord spot is set to collect a region transverse to the arc column starting 10 mm above the aeronautical sample. In addition, tens of shots were performed to determine the delay between the trigger of the spectrometer recording and the instant where the arc is passing the collecting spot. The spot size being higher than the cross section of the column itself, if the arc is not well collected by the optical system, the intensity of the spectrum has one or two orders of magnitude less than the a typical measurement. In those cases, the shot was rejected and the spectrum is not used.

3. Presentation of the swept-stroke phenomenon and arc channel elongation

3.1 Phenomenology of arc elongation and arc voltage evolution for RGE

During an RGE experiment, the arc hydrodynamics and electrical behaviours are governed by different phases. These different phases are described and detailed with the support of figures 6 and 7. Figure 6 represents images from the HSC of the different phases for a typical RGE experiment and figure 7 represents the associated arc voltage and current waveforms during the experiment. The arc current is 400 A. The test sample chord is 200 mm long. It has a speed of 49 m s^{-1} and has a cathodic polarity:

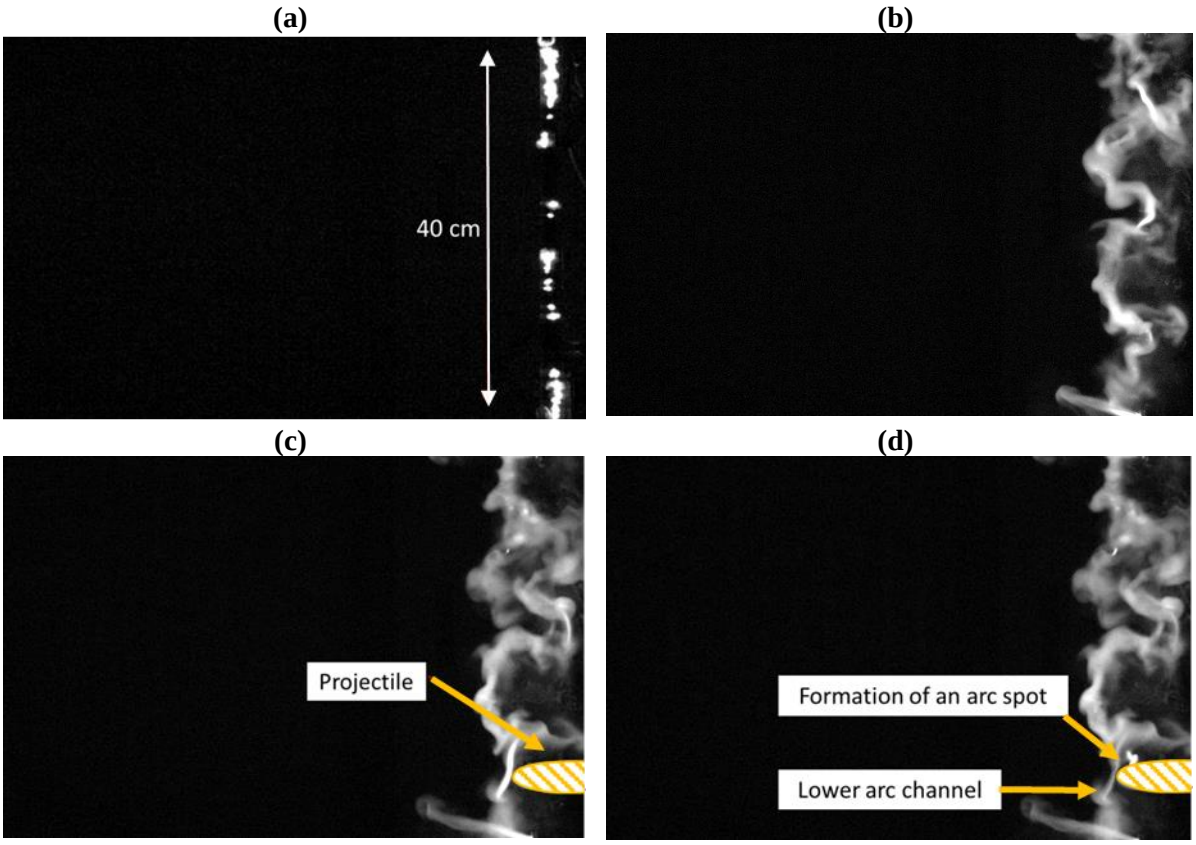

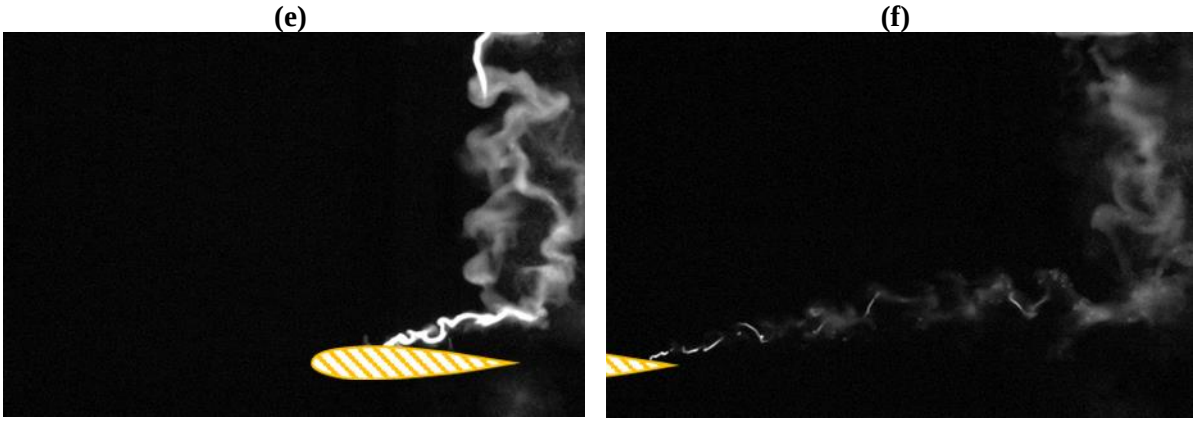

Figure 6. Successive images of the hydrodynamic behaviour of the arc channel during a RGE swept-stroke: (a) arc ignition phase, (b) static phase, (c) projectile arrival, (d) first strike (e) swept-stroke phase (f) arc extinction.

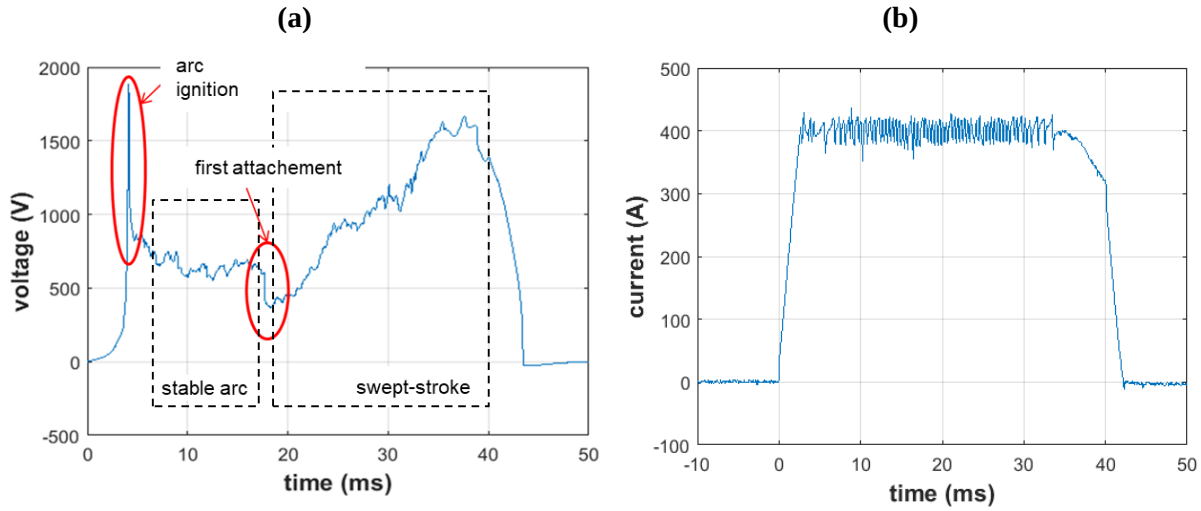

Figure 7. (a) Arc voltage and (b) current waveforms for the RGE.

The arc ignition phase: As described in Andraud et al. [24], the lightning arc is simulated with an indirect electrode configuration and thus an ignition wire of copper is used. This configuration is recommended by the standard guideline document ED-14E [29]. Due to the rise of current starting at 0 ms in figure 6(b), the arc is formed by the melting of a thin copper wire producing a plasma column that will sustain the discharge, as can be observed in figure 6(a). In this phase, the current is increasing rapidly and the arc voltage has a peak corresponding to the melting of the wire. The light emitted is becoming brighter due to the hot plasma column formation. The ignition phase lasts from 0 to 4.6 ms in figure 7(a) and is recognisable with its high voltage peak reaching 1950 V, which occurs at 4.1 ms.

The static phase: the electric arc is stable between the two static tungsten electrodes separated by 400 mm. Despite the distance between the two electrodes being constant, the length of the arc changes continuously due to the formation of current loops as a consequence of magnetic effects and due to thermal convection, as depicted in figure 6(b). However, the formation of new loops is compensated by the extinction of old loops so that the arc voltage remains globally constant. In figure 7(a), the static phase lasts from 4.6 to 17.6 ms and is characterised by a smooth voltage time variation of 100 V around a mean value of 650 V. The current is regulated at 400 A during this phase, as can be seen in figure 7(b).

The swept-stroke phase: the test sample crosses the electric arc. The arc reattaches the test sample that is connected to the lower electrode by a copper wire thus bypassing the arc channel initially formed below the sample, as can be seen in figures 6(c) and 6(d). The extinction of this lower arc channel, the length of which is approximatively 100 mm, provokes a voltage drop of several hundred volts that is observed in the arc voltage measurement. Indeed, in figure 7(a), at 17.6 ms, an abrupt voltage drop of 200 V occurs and corresponds to the first attachment of the arc channel on the material test sample. Then, as one arc root is stalled on the upper motionless electrode and the other arc root is involved in complex processes of dwelling and reattachment on the moving test sample, the electric arc is globally elongated, as can be observed in figure 6(e). In figure 7(a), the swept-stroke phase lasts from 17.6 to 40 ms and is characterised by a mean voltage increase from 380 to 1650 V and a current regulated to 400 A. Multiple arc extinctions and arc formations occur due to magnetic loop effects or to the reattachment of electric arc roots on the test sample. This might provoke occasional and sudden voltage drops. The global elongation of the arc during this phase generates the global increase in arc voltage despite the occurrence of some measured abrupt and marked voltage drops.

Arc elongation phase: when the arc root reaches the trailing edge, it cannot go any further on the surface of the test sample. This provokes arc elongation, because the test sample is still moving. The arc increases in size and then in voltage but there is no arc root reattachment on the test sample. Three main reasons can lead to an end of this elongation phase:

- The current regulation overshoots the 50 ms limit duration imposed on the lightning arc generator.
- The arc channel is so long that its voltage overshoots the capacitor voltage of the lightning generator.
- The arc manages to reattach on the initial motionless lower tungsten electrode

Arc extinction phase: At the end of the regulation – 50 ms – or when the arc voltage overshoots the lightning generator supply capacitor voltage, the current in the arc channel is slowly dropping and its light emission is fading away, as depicted in figure 6(f). The arc voltage remains at a constant value: the voltage measured between the electrodes no longer corresponds to the arc channel voltage but to the remaining capacitor voltage. In figure 7(a), the arc voltage reaches zero after the extinction: the capacitors have been drained of energy. Figure 7(b) shows that, after 33 ms, the generator is not able to provide a regulated current of 400 A: the current in the arc decreases until reaching zero within 10 ms.

3.2 Phenomenology of arc elongation and arc voltage evolution for WTE

During the experiment, the hydrodynamic and electrical behaviour of the arc is governed by almost the same different phases as RGE, as depicted in figures 8 and 9. Figure 8 represents HSC images of the different phases for a typical WTE experiment and figure 9 represents the associated arc voltage and current waveform during the experiment. The arc current is 400 A, the test sample is 200 mm long and has a cathodic polarity. The airflow velocity is 60 m s^{-1}.

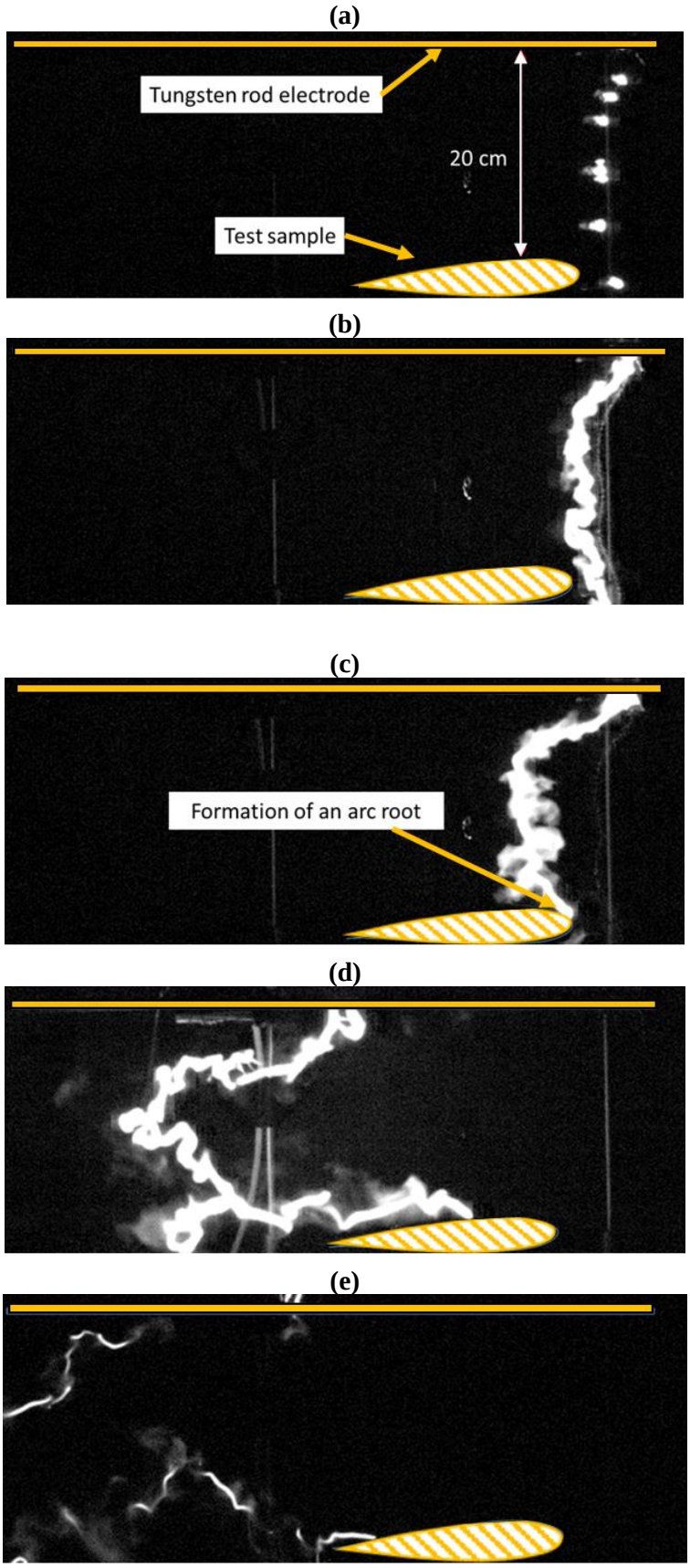

Figure 8. Successive images of the hydrodynamic behaviour of the arc channel during a WTE swept-stroke: (a) arc ignition phase, (b) static phase, (c) first strike (d) swept-stroke phase (e) arc extinction.

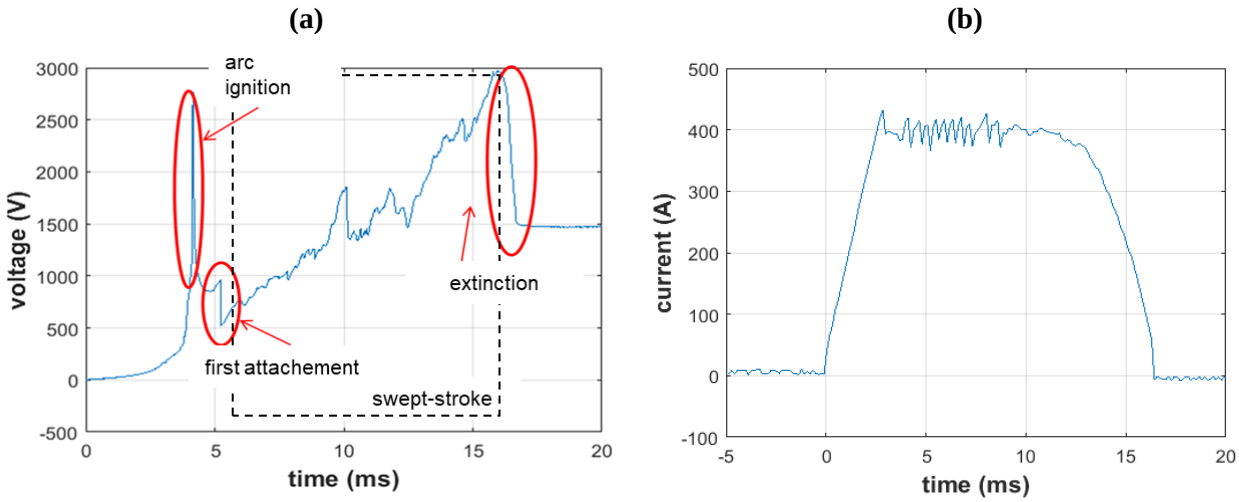

Figure 9. (a) Arc voltage and (b) current waveforms for the WTE.

The ignition phase: the arc is also formed by the melting of a thin copper wire due to the rise in current, observed in figure 9(b). However, as the wind tunnel is activated before the ignition, wire melting occurs while being blown by the airflow. Figure 8(a) shows that the wire is bending as it melts. In the example of figure 9(a), the ignition phase lasts from 0 to 4.4 ms and is recognisable with its high voltage peak reaching 2750 V occurring at 4.15 ms.

The static phase: as the arc column is blown from the instant it appears, it undergoes flexion since the extremities of the arc roots are less affected by the flow than the middle of the column, as is represented in figure 8(b). Thus, the arc channel is not static in this phase. The arc roots are moving in the flow direction so that the arc channel crosses the 50 mm that separate the ignition point from the leading edge of the test sample. The static phase lasts from 4.4 to 5.2 ms in the example of figure 9 and is characterised by a smooth voltage time variation of 100 V around a mean value of 870 V while the current is regulated at 400 A.

The swept-stroke phase: when the arc root first attaches to the test sample, the swept-stroke phase starts, as represented in figure 8(c). As for the static phase, the arc column seems to be blown by the airflow but the arc roots on the test sample and on the horizontal tungsten electrode are not displaced at the same speed as the column and are lagging behind. Thus, the arc column is outpacing the arc root, which moves either by reattachment processes or by continuous sweeping. This phenomenon is visible in figure 8(d). In figure 9(a), at 5.2 ms, an abrupt and marked voltage drop of 450 V occurs and corresponds to the first attachment of the electric arc on the material test sample. Then the swept-stroke phase lasts from 5.2 to 16.1 ms and is characterised by a mean voltage increase from 544 to 2973 V. The current value is regulated at 400 A, as depicted in figure 9(b).

Arc elongation phase: when the arc root on the test sample reaches the trailing edge, it cannot go any further and the arc is becoming expended because the arc channel is still blown by the transverse airflow.

Extinction phase: when the arc voltage overruns the generator voltage, the arc channel extinguishes because the generator cannot provide sufficient energy to maintain it. The current in the arc channel is dropping and its light emission is fading away, as can be seen in figure 8(e). In figure 9(b), after 16.1 ms, the capacitors cannot provide enough power to maintain the 400 A current regulation. In this configuration, the extinction phase directly follows the swept-stroke phase without the appearance of the arc elongation phase. Indeed, extinction occurs when the arc root has not yet reached the trailing edge of the sample. After extinction, figure 9(a) shows that the voltage is stable at 1500 V: the arc is extinguished and the voltage measured is that existing at the terminals of the capacitor bank.

It may be seen, in comparison with RGE, that the voltage reaches values two times higher at the end of the swept-stroke phase – 3000 V for WTE and 1500 V to 2000 V for RGE – and this increase is two times faster – 15 ms on average for WTE and 40 ms on average for RGE. Indeed, unlike RGE where only the part of the electric arc close to the attachment point is elongated, the whole arc column length is elongated with the airflow. Therefore, its length and thus its voltage increases more quickly.

The arc column geometry is also more complex for WTE than for RGE. In RGE, the arc channel has a straight, elongated shape during the swept-stroke phase. Conversely, in WTE, it is arcing and elongating along the airflow while the arc roots on the sample and on the horizontal tungsten rod electrode are lagging behind and slowly being pulled in the flow direction by the arc channel. The delay between the front arc column and the arc roots is increasing during the swept-stroke, as may be observed between figures 8(c) and 8(d).

4. Experimental results

4.1 Measurements of arc voltage slope and arc power variation

A good indicator of the arc elongation speed is the voltage slope (dU/dt) measured during the swept-stroke phase. Indeed, it is assumed that the arc voltage is proportional to its length, which is a parameter that is complicated to estimate with the images from the two cameras. Thus, the evolution of the arc voltage is considered to be the image of the evolution of arc length. For this reason, the voltage slope is measured from the arc voltage waveform for the swept-stroke phase and is chosen as a criterion to be discussed in this analysis. The voltage slope is defined as the slope between the first attachment and the arc detachment voltage or the end of the swept-stroke phase and it is measured directly from the arc voltage waveforms. For all the experiments with the railgun facility, the voltage slope is measured from the first reattachment on the test sample. The inter-electrode distance is set to 20 cm. The different voltage slopes for a same configuration of arc root polarity, current level, test sample speed and sample length are averaged and presented in figure 10. In figure 10(a), the distinction is made between cathodic (K) and anodic (A) arc spots and the speed indication is the average speed for two to four shots. In figure 10(b), the results for cathodic and anodic arc spots are averaged. For the majority of the shots, the chord of the test sample is 200 mm long. The results obtained with a 400 mm test sample chord are identified with an * after the speed indication. For both RGE and WTE, it is interesting to evaluate the arc power variation rate, which represents the variation in arc power during its elongation per unit of time, and is calculated by multiplying the current level by the arc voltage slope. This quantity is the image of the arc power evolution dynamic and its dependence on the input parameters is presented in figure 11. The results will be discussed in section 5.

(a)

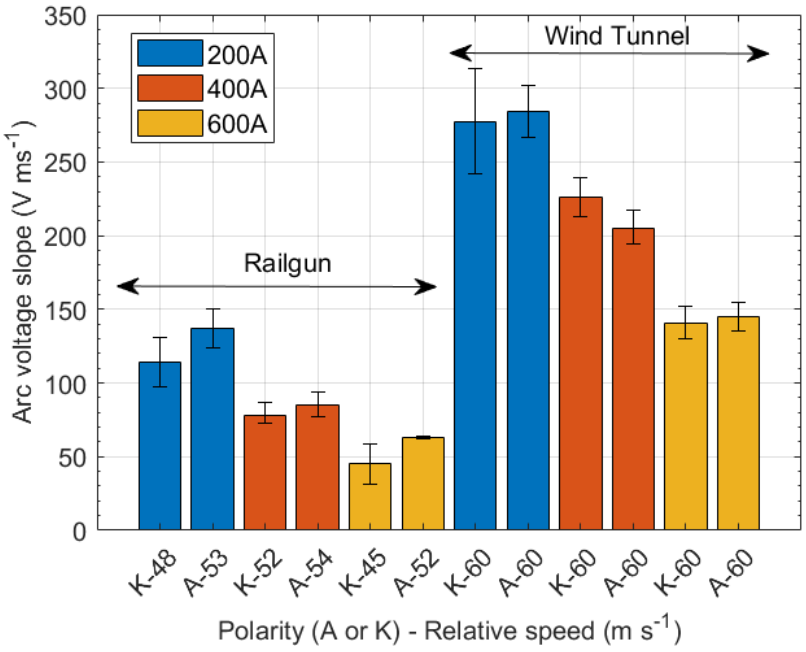

(b)

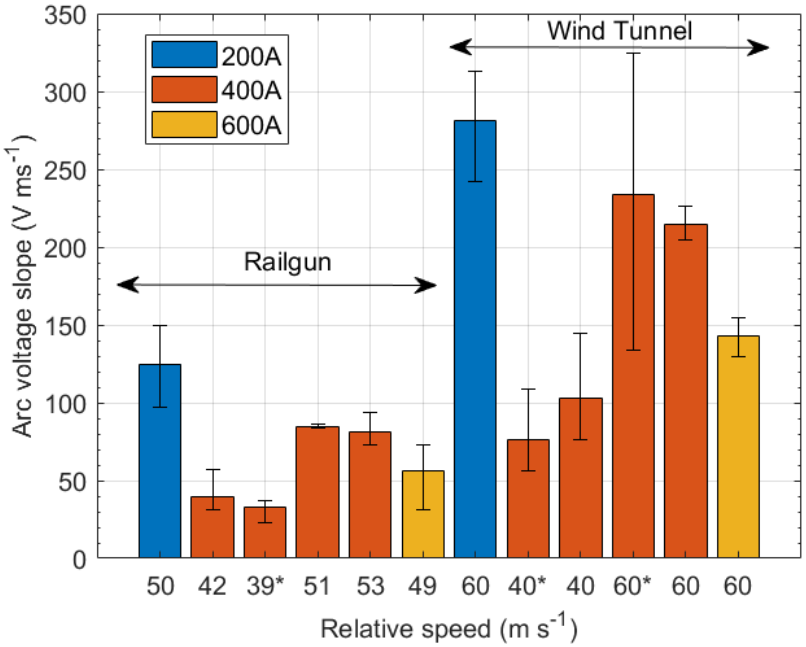

Figure 10. Arc voltage slope depending on (a) polarity, relative speed and current and (b) average relative speed, test sample chord length and current.

(a)

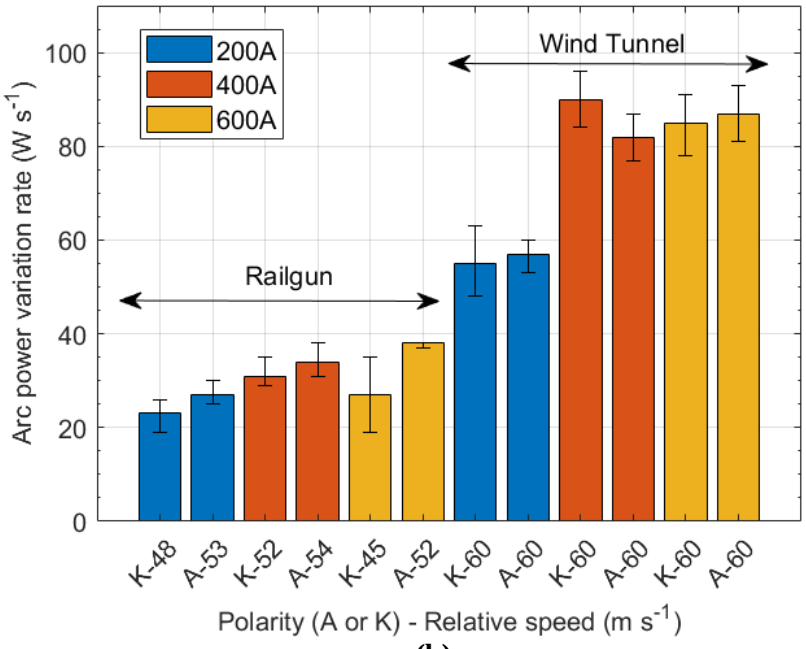

(b)

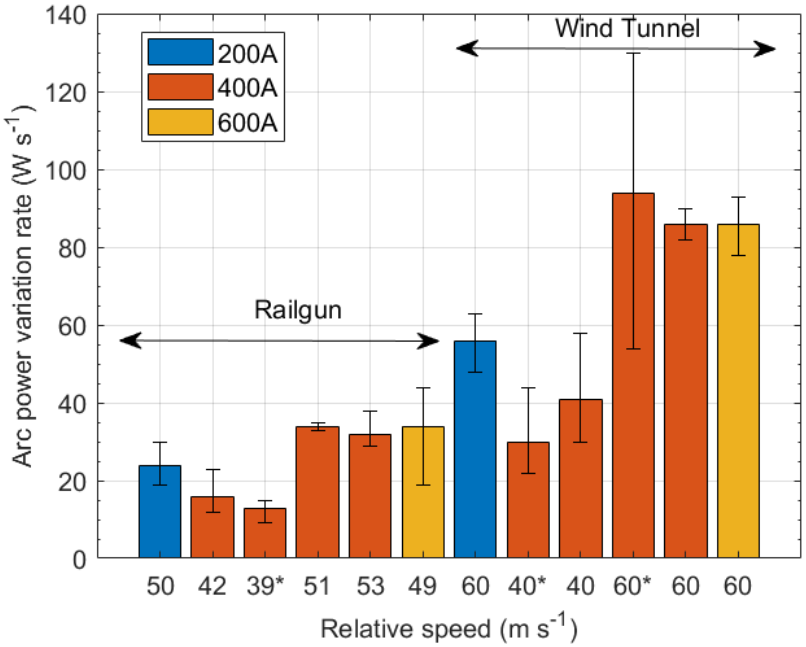

Figure 11. Arc power variation rate depending on (a) polarity, relative speed and current and (b) average relative speed, test sample chord length and current.

4.2 Optical emission spectroscopy measurements

The use of OES is a widely known and accepted technique for plasma diagnostics, and specifically for the thermodynamic characterisation of electric arcs. This technique has been specifically applied to lightning or electric arcs in different works: from welding arcs [30, 31] and natural lightning [32, 33] studies to in-lab pulsed lightning arc characterisation [34, 35]. In this work, we use the OES measurements to detect the main species emitting in the free arc column and in the region close to the

aeronautical sample. The identification of the main species allows us to estimate the arc column temperature based on the most resolved and intense lines.

4.2.1 Line emission and Boltzmann plot theory

Figure 12 presents an example of the acquired spectra for three cases (static free arc column, arc with Railgun and arc with wind tunnel) at a current level of 400 A.

The small amount of copper originating from the thin ignition wire significantly contaminates the electric arc so that the majority of the observed lines are from atomic copper (Cu I). This vapour contamination is likely to change the arc properties, in particular the transport and net emission coefficients, and so to alter the results [36]. However, the use of an ignition wire is the only configuration that makes it possible to initiate a metre-scaled electric arc in most current generators and this method is accepted by the lightning standard certification [5]. For a few cases (mostly in wind tunnel tests), we observed atomic oxygen (O I) and atomic nitrogen (N I) lines. A hydrogen Balmer-alpha line (Hα) is also observed in the spectra of the electric arc. Atomic hydrogen probably originates from the molecular dissociation of water vapour present in the laboratory and has also been reported in previous works [34].

(a)

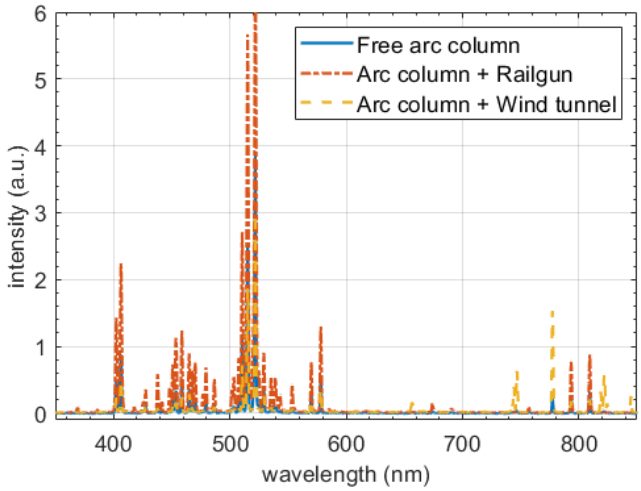

(b)

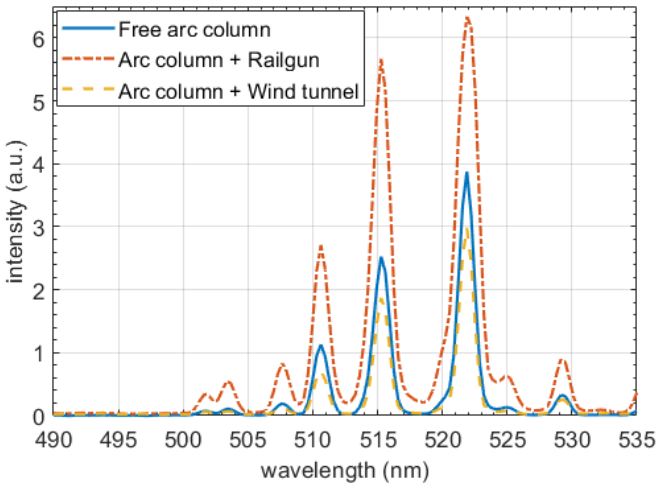

Figure 12. (a) Three spectra collected for the cases of a static free arc column, the arc with the electrode accelerated by the Railgun and the arc with an airflow generated by the wind tunnel. (b) Detail of copper lines around 515 nm.

The Boltzmann plot method is a well-known spectroscopic approach for plasma temperature characterisation. Two main hypotheses are assumed when applying this method: (i) the considered species are at local thermodynamic equilibrium (LTE) and (ii) the arc column is optically thin to those transitions. The radiation intensity $I(\lambda)$ along the chord collected by the optical system can be expressed from the optical energy balance between absorption and emission processes along the chord [37]. By considering the LTE assumption and using Kirchhoff's law, the ratio between the emission coefficient η and the absorption coefficient κ is equal to Planck's function I_λ^0. If the arc column is considered optically thin, we have the optical thickness $\kappa l \ll 1$, with l being the length crossed within the arc column. Then, the intensity $I(\lambda)$ collected by the optical system becomes directly proportional to the emission coefficient and the length l, resulting in the expression $I(\lambda) = \eta l$. The emission coefficient under LTE assumption and using the Boltzmann distribution can be expressed as:

$$\eta(\lambda) = \frac{hc}{4\pi} \frac{A_{ul}}{\lambda_{ul}} \frac{N_o(T, N_e)}{Q(T)} e^{-\frac{E_u}{kT}} f(\lambda - \lambda_{ul}) \quad (1)$$

where h and k are respectively Planck and Boltzmann constants, c is the speed of light, E_u and g_u are respectively the energy and the degeneracy of the upper transition level, A_{ul} is the Einstein emission coefficient for the transition from the upper (u) to the lower (l) level. N_o is the total population of the radiating species, which is a function of the temperature T and the electron density N_e, and Q is its internal partition function depending on T. λ_{ul} is the central wavelength and f is the normalized spectral line shape of the transition accounting for the broadening mechanisms.

The well-known expression of the Boltzmann plot method for a single transition is obtained by integrating (1) over the wavelengths:

$$\ln\left(\frac{\int I d\lambda}{\frac{g_u A_{ul}}{\lambda_{ul}}}\right) = -\frac{1}{kT} E_u + \ln\left(\frac{hc}{4\pi} \frac{N_o(T, N_e)}{Q(T)} l\right) \quad (2)$$

We observe that for each transition u to l, the integral of the line ($\int I d\lambda$) is directely correlated to the upper energy level E_u. Using different transitions and energy levels we can plot these points and use a linear regression to estimate the temperature from the angular coefficient. For the eleven observed lines, the spectroscopic constants in (2), E_u, g_u, A_{ul} and λ_{ul} were taken from the atomic spectral line database of NIST [38]. Table 1 presents the list of the considered lines with the corresponding spectrocopic data.

Table 1. Spectroscopic constants data used for the application of the Boltzmann plot.

λ_{ul} (nm)	g_u	A_{ul} (10^8s)	E_u(eV)
402.263	4	0.19	6.867
406.264	6	0.21	6.867
507.617	6	0.122	8.02
510.554	4	0.02	3.82
515.324	4	0.6	6.19
521.820	6	0.75	6.19
529.252	8	0.109	7.737
570.024	4	0.0024	3.817
578.213	2	0.0165	3.786
793.312	2	0.225	5.348
809.263	2	0.459	5.348

4.2.2 Temperature results

Figure 13 presents an example of the Boltzmann plot for a static free arc column of 400 A where a temperature of 11700 K is estimated. Generally, the measured data are well adjusted by linear regression from the Boltzmann plot method. A sensitivity analysis was performed to evaluate the influence of the less intense lines on the linear regression and consequently on the temperature determination. By comparing the results found using the Boltzmann plot with the eleven observed lines and with the temperature estimated using only the four most intense lines, we observed an average discrepancy of 500 K with a maximum of 1400 K. Table 2 summarises the results obtained for the studied cases, which cover different parameters between RGE and WTE.

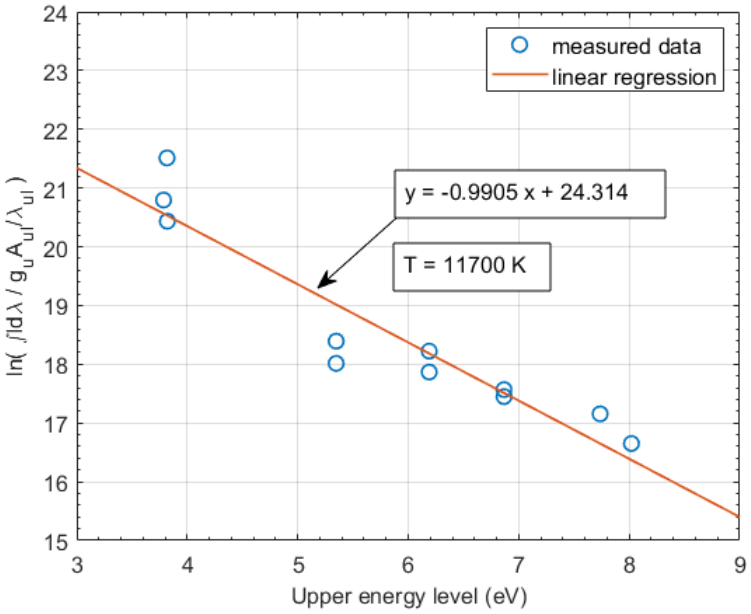

Figure 13. Example of the Boltzmann plot for a static free arc column of 400 A.

Table 2. Summary of the temperature results.

case	L (mm)	I (A)	Polarity	v (m s^{-1})	inter-electrode distance (mm)	T (kK)
Free arc	-	400	-	-	300	11.7
Free arc	-	400	-	-	300	11.3
RGE	200	400	K	55	200	11.7
RGE	200	400	K	42	200	10.8
RGE	200	400	A	45	200	10.5
RGE	400	400	K	37	200	10.5
RGE	200	200	A	54	200	9.2
RGE	200	200	A	52.5	200	9.5
RGE	200	600	K	40	200	12.9
RGE	200	600	A	50	200	13.3
RGE	200	600	A	54.5	200	13.0
WTE	200	400	K	60	200	11.4
WTE	200	400	K	40	200	10.5
WTE	400	400	K	40	200	10.8
WTE	400	400	K	60	200	12.3
WTE	200	200	K	60	200	8.2

5. Discussion

5.1 Effects of arc root polarity and relative speed on arc channel elongation

For RGE, the polarity of the moving arc root on the test sample does not seem to affect the spatial elongation, the voltage or the temperature of the arc channel. Indeed, for relative speeds between 45 and 55 m s^{-1}, the difference in arc voltage slope is at most 29% between a cathodic and an anodic arc root for the different current values. However, the systematic higher values of the anodic arc roots correlated with images of the swept-stroke are evidence of a different elongation process. In figure 14, the inclination angle is the angle between the arc column and the axis of the projectile movement, represented by a horizontal line. For the moving cathodic arc root, this angle is relatively high; the arc channel is globally bending to ensure arc connection to the test sample - as if the mechanical constraint applied by the arc root on the channel was distributed over the entire channel. Conversely, for the moving anodic arc root, the arc channel is not bending and rather exhibits a right angle between a motionless and straight arc column stalled between the two initial motionless electrodes and a column elongating in the direction of the projectile movement axis – as if only a restrained part of the column were supporting the arc root constraint. Thus, on the cathodic arc root, it is observed that as the entire arc channel is moving, the formation and elongation of the arc column is less necessary to ensure arc maintenance. On the anodic arc root, the maintenance of the arc between the moving and the motionless electrodes is ensured by the formation and the elongation of the arc column in the same direction as the axis of projectile motion so that its voltage slope needs to be higher on average – meaning that the length of the arc column is increasing more quickly. This difference can be partly explained by the difference in arc root dynamics depending on its polarity. Indeed, due to different emission processes, the anodic arc root is more likely to move freely on a metallic surface by reattachment processes whereas the cathodic arc root rather stalls at a point on a metallic surface [39].

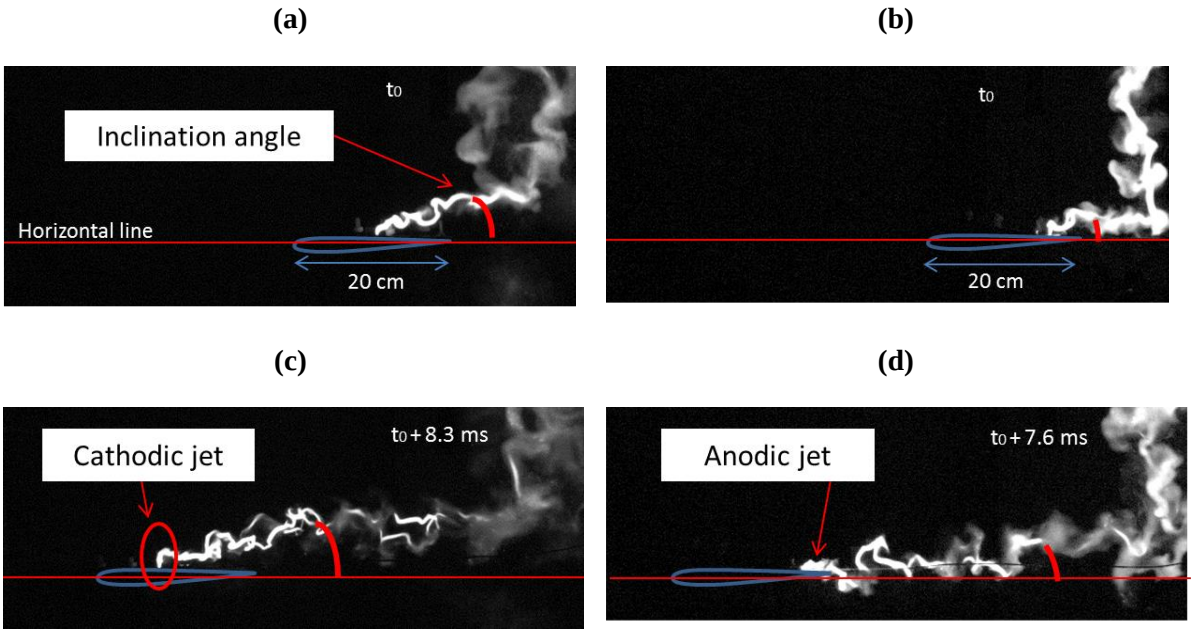

Figure 14. Different inclinations angles for: (a) moving cathodic arc root at the start and (c) the end of the swept-stroke phase, and (b) for moving anodic arc root at the start and (d) the end of the swept-stroke phase. It may be seen that the inclination angle between the arc channel and the horizontal line is more marked for the moving cathodic arc root. The stiffness of the cathodic jet is also observable.

Moreover, at low speed – 40 m s^{-1} – the difference in arc voltage evolution and arc behaviour during the swept-stroke phase is more marked between the cathodic and the anodic polarities. Indeed, no strong difference can be inferred from the voltage waveforms of cathodic and anodic polarities at 53 m s^{-1} since the two polarities exhibit a quite regular voltage slope during the entire swept-stroke. However, at 40 m s^{-1} the cathodic polarity exhibits a regular voltage slope during the swept-stroke phase, whereas the anodic polarity exhibits a voltage plateau before starting to increase. These differences can be observed in figure 15.

It can be observed with HSC that the plateau visible in figure 15(d) corresponds to successive attachments and restrikes on the test sample, for the anodic case at 40 m s^{-1}. At the end of the plateau – when the voltage starts to increase – the arc attaches to the trailing edge of the test sample and the arc is elongated due to the motion of the test sample. Therefore, no reattachment occurs after the end of the plateau and the swept-stroke phase is over. Since the arc voltage can be seen as the image of the arc length, it can be inferred for this case that the arc reattachment phenomenon balances out arc elongation due to the relative motion during the swept-stroke phase. In other words, the arc channel is not globally elongated since the swept-stroke process compensates arc stretching. This plateau is not observed for anodic test samples at 53 m s^{-1}, as shown in figure 15(b): the swept-stroke process is not sufficient to balance arc stretching and the arc column globally increases in length during the swept-stroke phase. The cathodic test sample experiments do not exhibit any plateau in their arc voltage waveform: this is mainly due to the different behaviour of the arc root on account of more complex physical processes. The cathodic arc root tends to stick and sweep on the test sample surface so that only a few reattachments are observed.

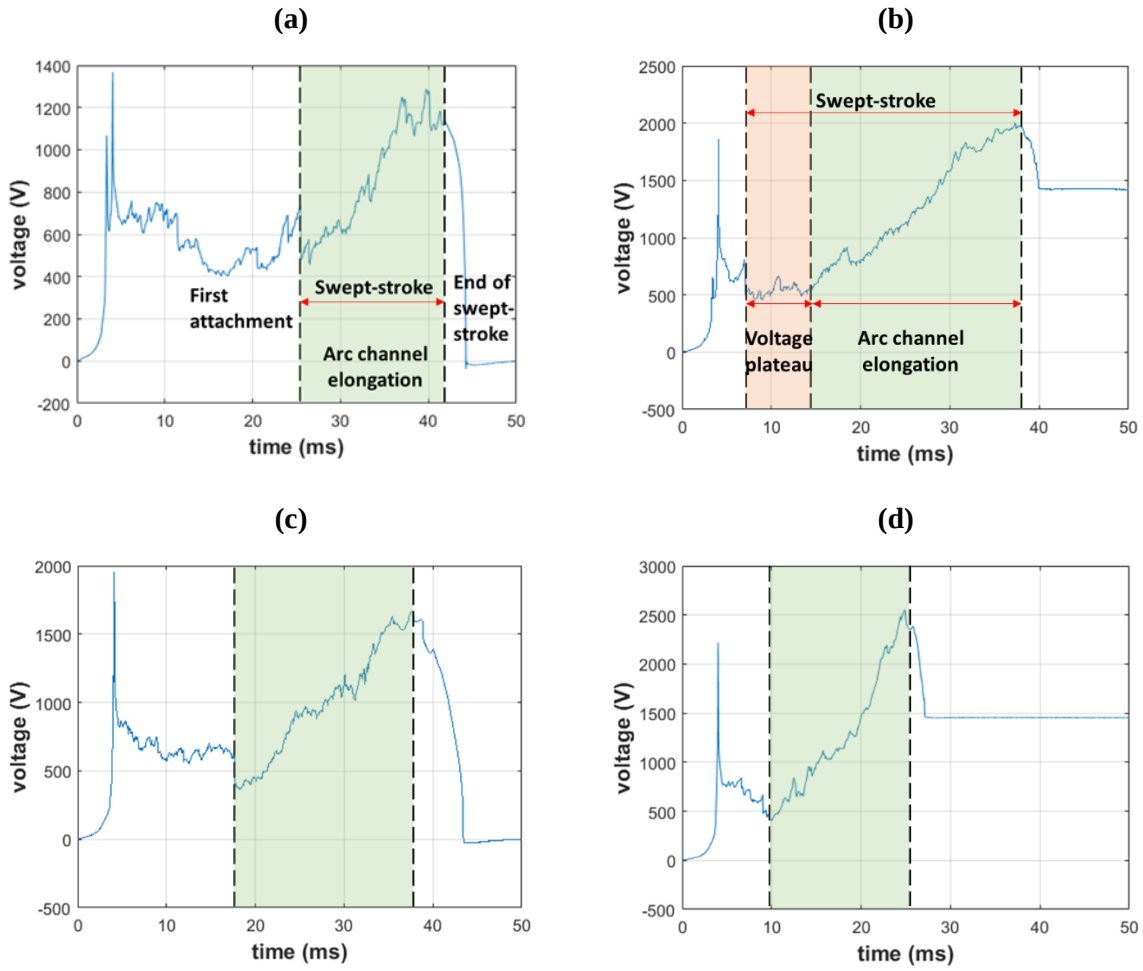

Figure 15. Differences in arc voltage evolution during swept-stroke for different speeds and polarity conditions: (a) cathodic at 50 m s^{-1}, (b) anodic at 53 m s^{-1} (c) cathodic at 42 m s^{-1} and (d) anodic at 38 m s^{-1}.

For WTE, this difference in behaviour between the cathodic and anodic arc roots is less marked for relative speeds between 40 and 60 m s^{-1} as the measured voltage slopes differ from 3 to 9%. Unlike RGE, no voltage plateau phase is observed in the arc voltage waveform for an anodic test sample at 40 m s^{-1}. It is still unclear if the absence or the presence of this plateau stems from a fundamental difference in physical processes for a relative motion due to a blown arc and due to a moving test sample. For WTE, the absence of this plateau in the arc voltage waveform may be due to the presence of another moving arc root on the upper electrode.

5.2 Effects of arc current on arc channel elongation

For both RGE and WTE, the results show that arc voltage slope for the swept-stroke phase is decreasing with increasing current level. Two main mechanisms can be considered to explain this variation in arc voltage slope:

The arc resistance varies with the current: according to Sousa Martins [40] and Chemartin [41], both the electrical conductivity and the diameter of the arc channel increase with the current level so that the arc channel resistance decreases with the increase in the arc current. According to the measurements of King [42], Tanaka *et al*. [43] and Sunabe and Inaba [44] and the simulation of C-waveform lightning arc of Chemartin [41], the electric field of the arc channel is independent of the level of arc current in this

current range. Thus, the variation in linear resistance with current level compensates the variation in current, as can be inferred from the equation:

$$E = r\,I \tag{3}$$

where E is the internal electric field of the arc channel and r the linear resistance. Thus, the electric power per unit of arc length, w, is given by:

$$w = E\,I = r\,I^2 \tag{4}$$

by assuming a constant E, the linear electric power (W m^{-1}) is a linear function of current resorting to (4) and so forming an equivalent length of arc column requires more energy for a 600 A arc channel than for a 200 A arc channel. This is in good agreement with the experimental measurements shown in figure 9: the arc voltage slope and therefor the elongation rate of the arc column decreases with the current – it requires more time for a 600 A arc channel to form a given arc length than for a 200 A channel. Therefore, it is interesting to discuss the arc power variation rate. The results show that the arc power variation rate is almost equivalent for the three current levels, even if it is 25% less for arcs of 200 A for RGE and 35% less for arcs of 200 A for WTE. This observation tends to demonstrate that the arc power evolution of the arc channel is driven by its spatial elongation, independently of the current level.

5.3 Effects of geometric conditions and the nature of relative motion on arc channel elongation

For both RGE and WTE, the length of the test sample does not seem to affect the arc voltage and spatial elongation. Indeed, the difference in the arc voltage slope between a test sample of 200 mm and 400 mm is 17.5% for RGE at 40 m s^{-1}, 9% for WTE at 60 m s^{-1} and 26% for WTE at 40 m s^{-1}. However, to ensure the representativeness of our tests considering in-flight lightning strikes with characteristic lengths of a few metres, larger test samples should be considered for future work.

For comparable experimental conditions between RGE and WTE – a relative velocity of 40 m s^{-1} and an arc current of 400 A – the arc voltage slope and the arc power variation rate are around 2.5 times higher for WTE than for RGE. One of the principal explanations is the presence of another moving arc root in the case of WTE that is also responsible for arc column elongation. The geometrical differences in arc channel are also very marked as previously discussed. Thus, the dynamics of arc spatial elongation and evolution of the arc energy are dramatically different even if more experiments have to be carried out to confirm this for other relative velocities.

5.4 Arc channel temperature

Generally, the effect of the current level on the temperature is well observed, as represented in figure 16. In the cases of 400 A the temperature is around 11 kK, regardless of the type of relative motion or even for the static free arc column. This increases to approximately 13 kK at 600 A and drops to values between 8.2 and 9.5 kK for 200 A. The effect of other parameters such as velocity, polarity or the type of relative motion cannot be clearly observed. Between different analysed cases, the temperature does not change more than 1000 K as a function of these parameters, which remains within the uncertainty of our measurements.

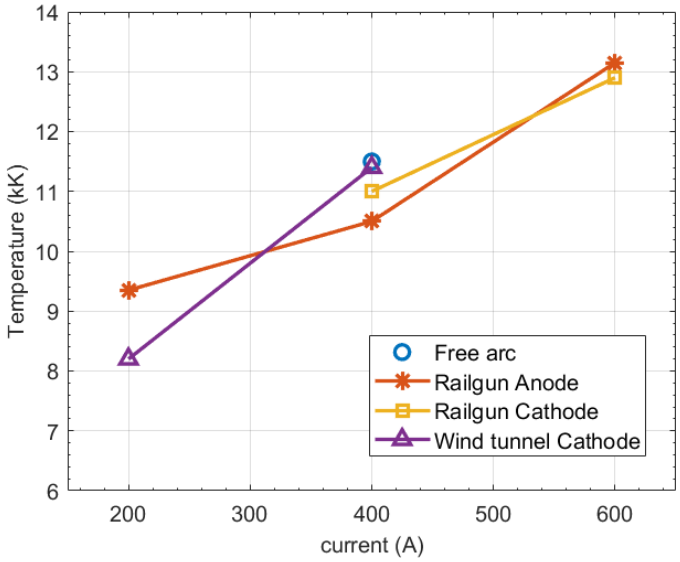

Figure 16. Results of temperature versus current level for different cases.

The order of magnitude of the temperatures obtained – around 11 kK – is in good agreement with the measurements of Valensi et al. [32] and Ma et al. [33], even if the spatial average that is performed by our collecting optical system may justify lower temperatures if compared to the expected values in the centre of the arc column. [32] also resorts to spectroscopy measurements combined with the Boltzmann plot method to characterise a welding arc in argon with a direct current of 330 A. [33] resorts to spectroscopy techniques to evaluate the temperature of a pulsed inert gas welding arc with a 200 A peak current and a pulse frequency of 5 Hz.

In general, this OES characterisation provides an order of magnitude for the arc temperature by assuming that the copper present in the arc column is at LTE. We observed that the current level has a general impact on the arc but the other parameters are likely to have only local influences, as in the sheath regions for instance. This could not be assessed with the present spectroscopic setup. Dedicated measurements with more accurate time and spatial resolution need be performed in further works to characterise these regions and investigate the influence of these additional parameters. Please also note that the assumption of LTE for the copper species as well as the influence of the copper in the thermo-physical properties of the arc may have an effect in the presented results.

6. Conclusions

A reference experimental database concerning the hydrodynamic, electrical and thermal properties of the arc channel during swept-stroke was established employing high-speed cameras, electric probe measurements and an optical emission spectroscopy technique. The coupling of the lightning arc generator with the railgun and the wind tunnel was successfully carried out with test samples having a NACA 0012 profile. The electrical and optical diagnostics were coupled to evaluate the arc channel elongation and the arc power evolution during swept-stroke.

For a moving test sample, launched with the railgun facility, the polarity of the moving arc root does not seem to influence the global elongation of the arc channel even if at 40 m s^{-1}, the anodic arc root reattachment process appears to neutralise the arc column elongation before the arc root reaches the trailing edge of the sample. It was also shown that arc channel elongation does not increase linearly with test sample speed. Arc power variation over time during arc elongation was estimated to be quasi-constant with the arc current level for a mean value of 30 W s^{-1} for an average speed of 53 m s^{-1}. The

test sample length and the initial arc column length did not demonstrate a noticeable influence on arc elongation.

For a moving electric arc, blown with the wind tunnel, the polarity of the arc root does not seem to influence the global elongation of the arc channel, either for different current and airflow velocity levels for a test sample of 200 mm. However, for a test sample of 400 mm, the global elongation manifestly differs between the cathodic and the anodic polarity. We also observed that arc channel elongation does not increase linearly with airflow velocity. Arc power variation over time during arc elongation was estimated to be also quasi-constant with the arc current level for a mean value of 76 W s^{-1} for an average speed of 60 m s^{-1}.

The mode of relative motion between the electric arc and the test sample dramatically affects arc elongation. Indeed, for a same value of test sample speed and airflow velocity of around 40 m s^{-1} , the electric arc exhibits an electric power variation and an arc elongation rate around 2.5 times higher for a moving electric arc with the wind tunnel than for a moving test sample with the railgun. This difference in hydrodynamic behaviour is confirmed by direct visualisation and is partially explained by the presence of a second moving arc root on the upper electrode and the non-uniform displacement of the arc channel induced by the airflow in the wind tunnel experiment. These results tend to demonstrate that swept-stroke simulations with moving arc and with moving sample are not equivalent in terms of physical processes. Consequently, since moving sample experiments are considered to be more representative of real lightning strikes, this mode of displacement should be preferred for designing further protection tests even if it is more difficult to implement technically.

An optical emission spectroscopy technique was employed to evaluate the electric arc temperature during swept-stroke. Generally, only the effect of the current level has a significant effect on the arc channel temperature, with a value around 9 kK for 200 A case and increasing up to 13 kK at 600 A. The effect of other parameters such as relative velocity, polarity, initial arc column length or the type of relative motion cannot be clearly identified.

For future work, the investigation of the temperature level inside the sheath regions could provide more results to analyse the physical processes occurring in the arc root during swept-stroke. Techniques of airflow visualisation are also considered for future work in order to provide insight into the complex interactions between the electric arc and the airflow during the phenomenon.

ACKNOWLEDGMENTS

The authors wish to thank the French Civil Aviation Authority (DGAC), France Relance and NextGenerationEU for their supports.

DATA AVAILABILITY

The data that support the findings of this study are available from the corresponding author upon reasonable request.

REFERENCES

[1] B. Fisher, R. Taeuber, and K. Crouch, *in AIAA 26th Aerospace Sciences Meeting, Reno, USA* (1988).

[2] C. Jones, D. Rowse, and G. Odam, *in Int. Conf. on Lightning and Static Electricity, Seattle, USA* (2001).

[3] J. A. Plumer, *in Int. Conf. on Lightning Protection, Vienna, Austria* (2012).

[4] SAE ARP5412A Aircraft Lightning Environment and Related Test Waveforms (2005).

[5] EUROCAE ED-84A Aircraft Lightning Environment and Related Test Waveforms (2013).

[6] B. Peyrou, L. Chemartin, Ph. Lalande, B. Cheron, Ph. Rivière, M.-Y. Perrin, and A. Soufiani, *J. Phys. D: Appl. Phys.*, **45**, 1455203 (2012).

[7] A. Larsson, P. Lalande, A. Bondiou-Clergerie, and A. Delannoy, *Journal of Physics D: Applied Physics*, **33**(15), 1866 (2000).

[8] A. Larsson, P. Lalande, and A. Bondiou-Clergerie, *Journal of Physics D: Applied Physics*, **33**(15), 1876 (2000).

[9] F. Tholin, L. Chemartin, and P. Lalande, *in Int. Conf. on Lightning and Static Electricity, Toulouse, France* (2015).

[10] J. A. Dobbing and A. W. Hanson, *in Int. Symp. on Electromagnetic compatibility*, Atlanta (1978).

[11] D. W. Clifford and L. E. McCrary, Final report: simulated lightning test Shuttle.03 scale model Report No. MDC A3155 McDonnell Aircraft Company, Saint Louis, Missouri (1974). available at https://ntrs.nasa.gov/citations/19760015187

[12] D. W. Clifford, K. E. Crouch, and E. H. Schulte, *IEEE Transactions on Electromagnetic Compatibility*, **2**, 209-224. (1982).

[13] L. L. Oh, and S. D. Schneider, *in Int. Conf. on Lightning and Static Electricity, Culham, UK* (1975).

[14] T. N. Meyer, *IEEE Transactions on Power Apparatus and Systems*, ***96***(4), 1324-1328 (1977).

[15] J. P. Novak, and V. Fuchs, *Proceedings of the Institution of Electrical Engineers* **121**, 1 (1974).

[16] P. Lalande, A. Bondiou-Clergerie, and P. Laroche, *in Int. Conf. on Lightning and Static Electricity, Toulouse, France* (1999).

[17] L. Chemartin, P. Lalande, B. Peyrou, A. Chazottes, P. Q. Elias, C. Delalondre, B. G. Cheron, and F. Lago, J. Aerospace Lab **5**, AL05-09 (2012), available at http://aerospacelab.onera.fr/al5/direct-effects-of-lightning-on-aircraft-structureanalysis-of-the-thermal-electrical-and-mechanical-constraints.

[18] P. L. Rustan, and J. P. Moreau, *in Int. Conf. on Lightning and Static Electricity, Paris, France* (1985).

[19] F. L. Pitts, and M. E. Thomas, "In flight direct strike lightning research", nasa_techdoc_19810010528, Document 10: 1981 00 I 0528, March (1981).

[20] J. C. Bailey, and R. V. Anderson, *Experimental Calibration of a Vector Electric Field Meter Measurement System on an Aircraft*. NAVAL RESEARCH LAB WASHINGTON DC (1987).

[21] J. Boulay, *Int. Conf. on Lightning and Static Electricity, Floride, USA* (1991).

[22] F. Uhlig, C. Jones, M. Vile, and Tagliana B, in *Int. Conf. on Lightning and Static Electricity*, Toulouse, *France* (1999).

[23] C. Guerra-Garcia, N. C. Nguyen, J. Peraire, and M. Martinez-Sanchez, *Journal of Physics D: Applied Physics*, ***49***(37), 375204. (2016).

[24] V. Andraud, R. Sousa Martins, C. Zaepffel, R. Landfried, and P. Testé, *Rev. Sci. Instrum.*, **92**, 104709 (2021).

[25] V. Andraud, R. Sousa Martins, C. Zaepffel, R. Landfried, and P. Testé, *Rev. Sci. Instrum.*, **93**, 084705 (2022).

[26] SAE ARP5412B Aircraft Lightning Environment and Related Test Waveforms (2013).

[27] EUROCAE ED-105A Aircraft Lightning Test Method (2013).

[28] V. Andraud, "Experimental implementation and study of the lightning swept-stroke along an aircraft". Ph.D. thesis, (Université Paris-Saclay, 2022).

[29] EUROCAE ED-14E Environmental Conditions and Test Procedures for Airborne Equipment (2011).

[30] J. Cen, P. Yuan, H. Qu, and T. Zhang, *J. Plasma Phys.*, **18**, 113506 (2011).

[31] Y. Mu, P. Yuan, X. Wang, and C. Dong, *J. Atmos. Sol. Terr. Phys.* **145** 98-105 (2016).

[32] F. Valensi, S. Pellerin, A. Boutaghane, K. Dzierzega, S. Zielinska, N. Pellerin, and F. J. Briand, *J. Phys. D: Appl. Phys.*, **43**, 434002 (2010).

[33] S. Ma, H. Gao, S. Zheng, and L. Wu, *J. Phys. D: Appl. Phys.*, **44**, 405202 (2011).

[34] R. Sousa Martins, C. Zaepffel, L. Chemartin, P. Lalande, and A. Soufiani, *J. Phys. D: Appl. Phys.*, **49**, 415205 (2016).

[35] R. Sousa Martins, C. Zaepffel, L. Chemartin, P. Lalande, and F. Lago, *J. Phys. D: Appl. Phys.*, **52**, 185203 (2019).

[36] Y. Liu, and Y. Wang, *IEEE Trans. Plasma Sci* **49**(5), 1661-1668 (2021).

[37] H. R. Griem, *Principles of Plasma Spectroscopy*. (Cambridge: Cambridge University Press, 1997).

[38] A. Kramida, Y. Ralchenko, J. Reader and NIST ASD Team (2021). NIST Atomic Spectra Database (ver. 5.9), [Online]. Available: https://physics.nist.gov/asd. National Institute of Standards and Technology, Gaithersburg, MD. DOI: https://doi.org/10.18434/T4W30F

[39] J.W. McBride, and P. A. Jeffery, IEEE Trans. Compon. Packag. Manuf. Technol, **22**(1) 38-46 (1999).

[40] R. Sousa Martins, "Experimental and theoretical studies of lightning arcs and their interaction with aeronautical materials". Ph.D. thesis, (Ecole Centrale Paris, 2016).

[41] L. Chemartin, "Modélisation des arcs électriques dans le contexte du Foudroiement des aéronefs". Ph.D. thesis, (Université de Rouen, 2008).

[42] L. A. King, *in Proceedings of the 5th Int. Conf. on Ionization Phenomena in Gases, Munich* (1961).

[43] S. Tanaka, K. Sunabe, and Y. Goda, *in 13th Int. Conf. on Gas Discharges and their applications, Glasgow* (2000).

[44] K. Sunabe, and T. Inaba, *Electr. Eng. Jpn.*, **110**(1), 9 (1990)